crystals

MDPI

Article

Mechanical and Tribological Properties of SPS-Sintered Y-TZP: The Effect of Sintering Temperature

Dávid Medveď, Jana Andrejovská * and Viktor Puchý

Institute of Materials Research, Slovak Academy of Sciences, Watsonova 47, 040 01 Kosice, Slovakia; dmedved@saske.sk (D.M.); vpuchy@saske.sk (V.P.)
* Correspondence: jandrejovska@saske.sk

Abstract

This work systematically investigates the influence of two spark plasma sintering (SPS) temperatures (1400 °C and 1600 °C) on the mechanical and tribological properties of two yttria-stabilized zirconia ceramics: 3 mol.% Y_2O_3 (3Y-TZP) and 1.5 mol.% Y_2O_3 (1.5Y-TZP). The ceramics' microhardness, nanohardness, Young's modulus, fracture toughness, and tribological performance were evaluated. The results show that 3Y-TZP maintains high hardness (Vickers hardness HV ~1300; nanohardness ~17.1 GPa) and stable fracture toughness (~4.2 MPa·m½), nearly independently of sintering temperature. In contrast, 1.5Y-TZP exhibits a critical trade-off: sintering at 1400 °C yields exceptional fracture toughness (~6.2 MPa·m½), but increasing the temperature to 1600 °C causes a sharp drop to ~4.5 MPa·m½. Tribologically, the highest wear resistance under a 5 N load was observed for the 3Y-TZP sample sintered at 1600 °C. These findings suggest that for low-yttria compositions, higher SPS temperatures can trigger detrimental microstructural changes that degrade toughness. The results provide crucial insights for tailoring SPS parameters and Y-TZP compositions for specific high-performance applications, balancing the competing requirements of hardness and fracture toughness.

Keywords: Y-TZP; spark plasma sintering (SPS); sintering temperature; mechanical properties; tribological properties; microstructure

check for updates

Academic Editor: Daisuke Nakauchi

Received: 29 May 2025
Revised: 10 June 2025
Accepted: 18 June 2025
Published: 23 June 2025

Citation: Medveď, D.; Andrejovská, J.; Puchý, V. Mechanical and Tribological Properties of SPS-Sintered Y-TZP: The Effect of Sintering Temperature. *Crystals* **2025**, *15*, 593. https://doi.org/10.3390/cryst15070593

Copyright: © 2025 by the authors. Licensee MDPI, Basel, Switzerland. This article is an open access article distributed under the terms and conditions of the Creative Commons Attribution (CC BY) license (https://creativecommons.org/licenses/by/4.0/).

1. Introduction

Zirconia-based ceramics, particularly yttria-stabilized tetragonal zirconia polycrystals (Y-TZPs), are among the most important structural materials due to their exceptional combination of mechanical strength, hardness, fracture toughness, chemical stability, wear resistance, and biocompatibility [1–4]. Due to these favorable properties, Y-TZP ceramics can be employed in a broad spectrum of advanced structural and functional capacities, including use as dental implants and restorations [5,6], cutting tools, bearings, seals, and other components exposed to severe wear conditions, such as in demanding wear applications and gas turbines [7].

The high fracture toughness of Y-TZP is primarily attributed to transformation toughening—the ability of metastable tetragonal ZrO_2 (t-ZrO_2) grains to transform to the monoclinic phase (m-ZrO_2) in the vicinity of a crack tip under applied stress. This martensitic transformation is accompanied by a volumetric expansion (approximately 3–5%), generating compressive stresses that hinder further crack propagation [8,9]. The effectiveness of this mechanism and the resulting properties of the ceramic are closely

related to microstructural features like density, average grain size, and phase composition, governed by powder composition (especially the Y_2O_3 content) and consolidation conditions, particularly the sintering process [2,4,10]

Conventional sintering methods for Y-TZP often require high temperatures (1450–1600 °C) and long dwell times to achieve near-theoretical density, but this typically leads to excessive grain growth and reduced stability of the tetragonal phase [11]. As an alternative, spark plasma sintering (SPS), also known as the field-assisted sintering technique (FAST), has emerged as an advanced method for the rapid consolidation of ceramic powders [12–14]. SPS combines uniaxial pressure with a direct pulsed electric current, enabling extremely rapid heating rates and short dwell times. This allows for full densification and the formation of a fine-grained microstructure at significantly lower temperatures. These benefits are crucial for preserving submicron grain dimensions and optimizing the mechanical behavior of Y-TZP ceramics [13,15]. The kinetics of densification, diffusion, grain growth, and phase stability are governed by a set of critical SPS parameters [4,14,16]. These primarily include the sintering temperature, applied pressure, heating rate, and dwell time. An insufficient sintering temperature may result in residual porosity and degraded mechanical properties, while an excessive temperature causes uncontrolled grain growth and destabilization of the tetragonal phase [10,17]. The stabilizer content, particularly that of Y_2O_3, is equally crucial: lower yttria concentrations (e.g., 1.5 mol.%) enhance transformation toughening capability but require precise process control to prevent spontaneous t→m transformation and to ensure a fine-grained microstructure [4,18–20]. Powder pre-processing (e.g., milling) also has a significant effect on powder reactivity and microstructural homogeneity [15].

Despite numerous studies on Y-TZP, the complex interplay among sintering parameters, the yttria content, and, critically, the resulting tribological performance under varying loads remains incompletely understood. Specifically, the dominant wear mechanisms—such as abrasion, plastic deformation, or phase transformation-induced microcracking—and how they shift with changes in microstructure are still debated, especially for materials consolidated by advanced methods like SPS [6,19,21]. Furthermore, as zirconia finds new applications in extreme environments, such as in functional components in nuclear reactors, understanding its long-term stability becomes paramount [22,23].

The novelty of this work lies in directly addressing this gap. We provide a systematic, side-by-side comparison of a low-yttria (1.5 mol.%) and a standard (3 mol.%) composition processed at two distinct SPS temperatures (1400 °C and 1600 °C). By correlating comprehensive mechanical data (hardness, toughness, modulus) with detailed tribological results under multiple loads, this study aims to elucidate the critical trade-offs between wear resistance and fracture toughness. Our integrated approach provides new, application-oriented insights for tailoring Y-TZP ceramics for specific high-stress environments where either maximum durability or fracture tolerance is the primary design driver.

2. Materials and Methods

2.1. Materials Preparation and Processing

Commercially available powders were used as starting materials: tetragonal ZrO_2 stabilized with 3 mol.% Y_2O_3 (3Y-TZP; Tosoh Corporation, Tokyo, Japan, 0.04 µm particle size) and pure ZrO_2 powder (Alfa Aesar, Karlsruhe, Germany, 1 µm particle size). To prepare a powder mixture with a target composition of 1.5 mol.% Y_2O_3 (1.5Y-TZP), pure ZrO_2 powder was added to the 3Y-TZP powder in a stoichiometrically calculated mass ratio. This approach was chosen to ensure that the baseline characteristics of the stabilized zirconia particles were identical for both compositions, allowing for a more direct comparison of the effect of yttria content.

Both powder mixtures (3Y-TZP and 1.5Y-TZP) were homogenized by dispersing each mixture in isopropanol (approximately 40 vol.% solids) and milling it in a planetary ball mill (PM 100, Retsch, Haan, Germany) for 2 h at a rotation speed of 200 rpm. The milling was performed using a zirconia milling jar and balls, with a ball-to-powder weight ratio of 10:1. To ensure a uniform particle distribution and prevent agglomeration, the milling direction was reversed every 30 min. After milling, the suspension was evaporated using a rotary evaporator; the resulting powder was dried in an oven at 80 °C for 12 h and subsequently sieved through a 200 µm mesh. The prepared and homogenized powders were stored in a desiccator until further processing to prevent moisture absorption.

The powder mixtures were consolidated using spark plasma sintering (SPS) in an HP D10-SD system (FCT Systeme GmbH, Effelder-Rauenstein, Germany). The powder was loaded into a graphite die with an inner diameter of 20 mm, lined with a 0.5 mm thick graphite foil to prevent reactions between the powder and the die and to facilitate sample removal. The sintering cycle was as follows:

- Preheating: A linear ramp to 400 °C was applied at 100 °C/min, followed by a 2 min dwell to eliminate residual moisture and adsorbed gases.
- Main heating: Heating from 400 °C to the target sintering temperature (1400 °C or 1600 °C) at a rate of 100 °C/min.
- Isothermal hold: At 1400 °C, a dwell time of 5 min; at 1600 °C, the dwell time was reduced to 4 min.
- Cooling: After the isothermal hold, controlled cooling to 400 °C at 100 °C/min, followed by free cooling to room temperature in the device chamber.

The application of pressure during the SPS cycle depended on the target sintering temperature. For sintering at 1600 °C, uniaxial pressure corresponding to a force of 20 kN (approximately 64 MPa) was applied starting at 400 °C and maintained throughout heating, the isothermal hold, and the initial cooling phase. In contrast, for sintering at 1400 °C, the pressure was applied gradually as the temperature increased, with the full 20 kN force reached only at the target sintering temperature. The rationale for the gradual pressure application at 1400 °C was to ensure complete outgassing before final densification. While the authors acknowledge that this variation in pressure profiles constitutes a limitation of the study, it is argued that the 200 °C difference in sintering temperature is the overwhelmingly dominant factor governing the final material properties, as discussed further in Section 4.

The sintering technique resulted in cylindrical samples with a diameter of 20 mm and a height of approximately 4 mm. The bulk density of the sintered samples was evaluated via the Archimedes method using distilled water as the immersion fluid, in compliance with ISO 18754 [24].

A closer examination of the time-dependent SPS curves (Figure 1) allows a more detailed interpretation of the densification process and its influence on the resulting microstructure. The initial rapid heating ramp up to 400 °C is intended primarily for the removal of residual moisture and adsorbed gases, helping to prevent undesired porosity. The subsequent main heating phase up to the target sintering temperature (1400 °C or 1600 °C) at 100 °C/min marks the onset of intensive densification, as clearly indicated by the pronounced decrease in piston displacement on the SPS curve. This segment corresponds to particle rearrangement, plastic deformation, and the onset of diffusion-driven neck formation, which are crucial for achieving high density and uniformity. The brief isothermal hold at the peak temperature (4 or 5 min, depending on the sintering protocol) enables the completion of densification and stabilization of the microstructure, with simultaneous application of uniaxial pressure (up to 64 MPa) supporting mass transport while restricting excessive grain growth.

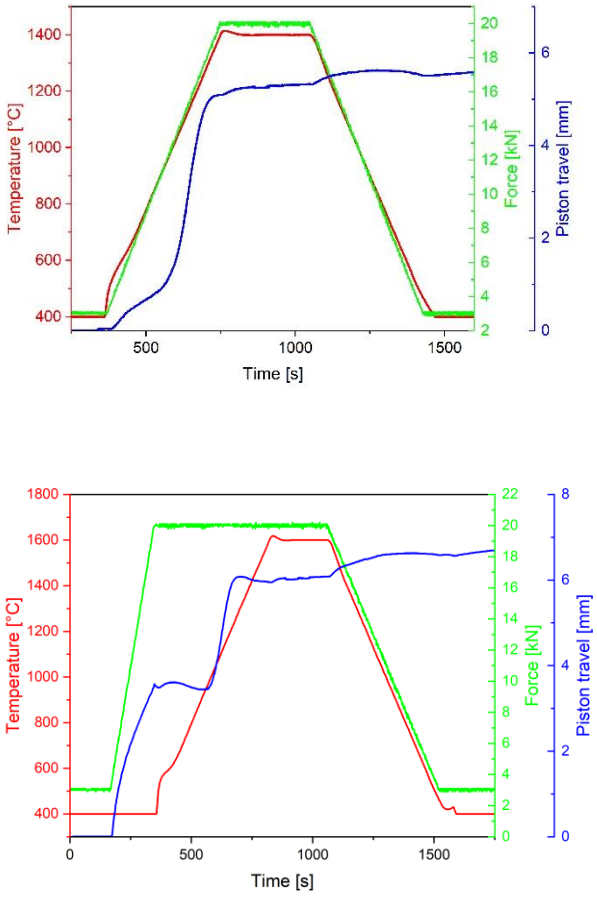


Figure 1. Time-dependent temperature and pressure curves during the SPS cycle in both operating modes.

Controlled cooling to 400 °C minimizes residual thermal stresses, and the gradual pressure release during cooling is designed to avoid sample cracking. The slightly different pressure application profiles between the two sintering temperatures are reflected in the SPS curves and may contribute to subtle microstructural variations, as discussed in Section 4.

Overall, these SPS curve segments directly illustrate how rapid heating, densification under pressure, short isothermal holding, and controlled cooling each play a critical role in producing high-density, fine-grained Y-TZP ceramics.

2.2. Characterization and Testing Methods

For microstructural analyses and mechanical testing, the surfaces of the sintered samples were prepared using standard metallographic procedures. This involved coarse grinding on SiC papers with grit sizes progressing from 320 to 1200, followed by fine polishing with diamond suspensions of 9 µm, 3 µm, and 1 µm particle sizes. The quality of the prepared surfaces was verified by measuring the surface roughness using a confocal microscope (Sensofar PLu Neox, Sensofar Metrology, Barcelona, Spain). The achieved average arithmetic surface roughness (Ra) was approximately 0.06 µm.

The morphology and microstructure of the sintered samples were examined using environmental scanning electron microscopy (SEM, EVO MA15, Carl Zeiss, Jena, Germany). The analysis was performed in backscattered electron (BSE) mode, which provides contrast based on the chemical composition.

The Vickers microhardness was measured using a Vickers hardness tester (432SVD, Wolpert Wilson Instruments, Lake Bluff, IL, USA). For most samples, a load of 98.1 N (HV10) was applied. For the 1.5Y-TZP sample sintered at 1400 °C, a load of 49.05 N (HV5) was used. This deviation was due to an evolution in the experimental protocol

between measurement series. To verify the comparability of the results, preliminary tests on the 3Y-1400 sample were conducted at both loads, yielding highly consistent values (1362 HV5 versus 1337 HV10). Given this minimal load dependence, the use of HV5 for this specific sample is considered to have a negligible impact on the overall comparability of the hardness data. The dwell time of the indenter was 15 s for all measurements. For each sample, at least five valid indents were made, with sufficient spacing between them and from the sample edges. The Vickers hardness was determined according to Equation (1):

$$HV = 0.189 \cdot \left(\frac{P}{d^2} \right) \quad (1)$$

where P is the applied load (N) and d is the arithmetic mean of the diagonals of the indentation (mm).

Nanoindentation tests were performed on an Agilent G200 instrument (Agilent Technologies, Santa Clara, CA, USA) equipped with a Berkovich diamond tip. A matrix of 100 indents (e.g., 5 × 5) with a maximum indentation depth of 1200 nm was made on each sample. Measurements were carried out in Continuous Stiffness Measurement (CSM) mode. The values of the Young's modulus and nanohardness were calculated automatically by the instrument's software (version 6.54) based on the Oliver–Pharr method [25]. Tip calibration was performed before measurement using a fused silica reference sample.

The indentation fracture toughness (K_{IC}) was determined from the lengths of the radial cracks generated at the corners of the Vickers indents during the microhardness measurements.

The calculation was performed using the Anstis equation, Equation (2) [26]:

$$K_{IC} = 0.016 \cdot \left(\frac{E}{H} \right)^{1/2} \cdot \frac{P}{c^{3/2}} \quad (2)$$

where E is the Young's modulus (GPa), H is the Vickers hardness (GPa), P is the applied load (N), and c is the radial crack length (μm). The value of the Young's modulus (E) required for the calculation was obtained from nanoindentation measurements.

Tribological properties were evaluated using a universal tribometer (Bruker UMT-3, Bruker Corporation, Billerica, MA, USA) in a ball-on-flat configuration with linear reciprocating motion. The counterbody was a 6 mm diameter SiC ball. Tests were performed under dry conditions at room temperature (22 ± 1 °C) and a relative humidity of 40 ± 5%. The test parameters were as follows: stroke amplitude of 5 mm, frequency of 10 Hz, corresponding to an average sliding speed of 0.1 m/s. Three different normal loads were applied: 5 N, 10 N, and 25 N. The total sliding distance for each test was 500 m. The coefficient of friction was continuously recorded throughout the test. After tribological testing, the wear volume and morphology of the wear track were analyzed. The volume of material removed (V) was determined from the 3D topography of the wear track measured by a confocal microscope (Sensofar PLu Neox, Barcelona, Spain). Based on the measured wear volume, the specific wear rate (Ws) was calculated according to the following equation:

$$Ws \frac{V}{F_N.L} \left[\frac{\text{mm}^3}{\text{Nm}} \right] \quad (3)$$

where F_N is the normal load, L is the sliding distance, and V is the volume of material removed after wear.

The morphology of the wear track, wear mechanisms, and presence of any tribolayers were analyzed in detail using scanning electron microscopy (SEM). Observations were performed in both secondary electron (SE) and backscattered electron (BSE) modes. The

chemical composition of the surfaces and any tribolayers was analyzed by an energy-dispersive X-ray spectroscopy (EDX) device integrated into the SEM instrument.

3. Results

3.1. SPS Sintering Behavior

The densification behavior during the SPS process is illustrated by the sintering curves in Figure 1. For both temperature profiles, the main densification, indicated by the sharp increase in piston travel (blue curve), initiates at approximately 850 °C and accelerates significantly above 1100 °C. This corresponds to the onset of major diffusion-driven neck formation. At 1400 °C (left plot), densification appears to be nearly complete when the holding temperature is reached, as the piston travel plateaus. At 1600 °C (right plot), a slightly greater final piston displacement is observed, suggesting that the higher thermal energy promotes further particle rearrangement and plastic flow.

The course of spark plasma sintering (SPS) was monitored by recording the temperature, applied force, and piston displacement as a function of time. For all cycles, the main densification phase occurred in the 800–1400 °C interval, as evidenced by a pronounced decrease in the height of the powder bed.

The bulk densities and corresponding relative densities of the sintered samples are summarized in Table 1. The theoretical densities used for calculation were 6.08 g/cm^3 for 3Y-TZP and 6.11 g/cm^3 for 1.5Y-TZP. All samples achieved high relative densities (>96%). The 3Y-TZP samples reached slightly higher densities than did the 1.5Y-TZP samples. The effect of sintering temperature was not monotonic; for 3Y-TZP, the density slightly increased with temperature, whereas for 1.5Y-TZP, it slightly decreased, a finding that will be addressed in the Discussion.

Table 1. Density of individual samples.

Sample	Density [g/cm^3]
3Y-1400	6.03 ± 0.02
1.5Y-1400	5.90 ± 0.03
3Y-1600	6.05 ± 0.01
1.5Y-1600	5.86 ± 0.05

3.2. Mechanical Properties

An overview of the main mechanical parameters is provided in Table 2.

Table 2. Microhardness (HV), fracture toughness (K_{IC}), nanohardness (H_{IT}), and Young's modulus (E_{IT}) for each sample.

Sample	Microhardness HV	Fracture Toughness K_{IC} [MPa·m^{½}]	Nanohardness H_{IT} [GPa]	Young's Modulus E_{IT} [GPa]
3Y-1400	1337 ± 12 (HV10)	4.24 ± 0.03	17.27 ± 0.51	258.1 ± 5.4
3Y-1600	1319 ± 21 (HV10)	4.21 ± 0.04	17.11 ± 0.75	250.8 ± 9.0
1.5Y-1400	974 ± 18 (HV5)	6.24 ± 0.46	12.47 ± 0.86	219.5 ± 6.9
1.5Y-1600	968 ± 12 (HV10)	4.48 ± 0.16	13.79 ± 1.25	238.8 ± 11.1

- Increasing the sintering temperature from 1400 °C to 1600 °C did not lead to significant changes in microhardness or nanohardness for 3Y-TZP, but for 1.5Y-TZP, a slight increase in nanohardness was observed, accompanied by a decrease in fracture toughness.

- The highest fracture toughness (K_{IC}) was observed in the 1.5Y-1400 sample.
- The 3Y-TZP materials exhibited higher hardness and Young's modulus values compared to 1.5Y-TZP.

3.3. Tribological Properties

Table 3 summarizes the coefficient of friction (COF) and wear rate (Ws) values for each sample and applied load.

Table 3. Coefficient of friction (COF) and wear rate (Ws) at different loads.

Sample—Sintering Temp [°C]	Load [N]	COF [-]	Ws [mm^3/Nm]
1.5Y-TZP—1400	5	0.386	2.52×10^{-7}
	10	0.377	4.18×10^{-7}
	25	0.355	3.96×10^{-7}
1.5Y-TZP—1600	5	0.400	1.76×10^{-7}
	10	0.379	2.87×10^{-7}
	25	0.360	5.02×10^{-7}
3Y-TZP—1400	5	0.392	5.06×10^{-8}
	10	0.383	3.28×10^{-7}
	25	0.374	4.59×10^{-7}
3Y-TZP—1600	5	0.410	4.80×10^{-8}
	10	0.390	3.20×10^{-7}
	25	0.370	5.38×10^{-7}

- For all samples, a slight decrease in the COF was observed with increasing load.
- The lowest wear rate at 5 N was achieved by the 3Y-1600 sample.
- At higher loads, the differences in wear rates between the materials diminished. Notably, at 25 N, the wear rates were all within the same order of magnitude, although the 1.5Y-TZP sample sintered at 1400 °C (3.96×10^{-7} mm^3/Nm) still showed slightly better performance than its counterpart sintered at 1600 °C (5.02×10^{-7} mm^3/Nm).

3.4. Tribological Surface Characterization

The surface features of wear tracks after tribological testing (Figure 2) were thoroughly analyzed by scanning electron microscopy (SEM) and energy-dispersive X-ray spectroscopy (EDX) to identify the dominant wear mechanisms for each material and testing condition.

In general, all examined samples exhibited an abrasive wear mechanism, manifested by pronounced grooves and scratches oriented in the sliding direction. The intensity of abrasive damage increased with increasing normal load. The EDX analysis confirmed a key phenomenon—the transfer of material from the SiC counterbody to the surface of the zirconia samples. This transferred SiC appeared as darker areas in SEM images and played a significant role in further wear, likely acting as a third-body abrasive medium.

For the 3Y-TZP sample sintered at 1400 °C (3Y-1400), we observed the following:

- At low load (5 N), the wear track was characterized by fine abrasive grooving and scattered, discontinuous patches of transferred SiC. The track edges were clean, without significant accumulation.
- With increasing load (10 N and especially 25 N), SiC transfer became more massive, forming a thicker and uneven layer, more concentrated at the track edges. This layer tended to crack and delaminate, resulting in more intensive abrasive wear.

For the 3Y-TZP sample sintered at 1600 °C (3Y-1600), we observed the following:

- At 5 N, fine abrasive wear dominated, with longitudinal bands of transferred SiC mainly at the track edges.
- At 10 N, the extent of SiC transfer increased and the abrasive grooves in the zirconia matrix were deeper.
- At 25 N, the wear track was almost entirely covered by a thick, fragmented, and severely damaged SiC layer, which exhibited fragmentation and delamination, leading to intense abrasive wear.

The 1.5Y-TZP samples behaved differently, likely due to their lower hardness:

- For 1.5Y-TZP sintered at 1400 °C (1.5Y-1400), even at 5 N load, extensive, fragmented SiC transfer was observed, covering a significant portion of the track, along with pronounced abrasive grooving of the matrix.
- At 10 N, the intensity of these phenomena increased.
- At 25 N, the surface morphology was highly destructive, with massive, chaotic SiC transfer forming an extremely unstable, porous, and fragmented layer.

The 1.5Y-TZP sample sintered at 1600 °C (1.5Y-1600) showed the following:

- At 5 N, it exhibited a practically identical worn surface morphology to the 1.5Y-1400 sample, with discontinuous patches of transferred SiC and abrasive grooving.
- At 10 N, SiC transfer was more extensive, and the abrasive grooves were deeper.
- At 25 N, the surface layer was again highly destructive, with massive SiC transfer, fragmentation, and delamination—similar to that for the 1.5Y-1400 sample.

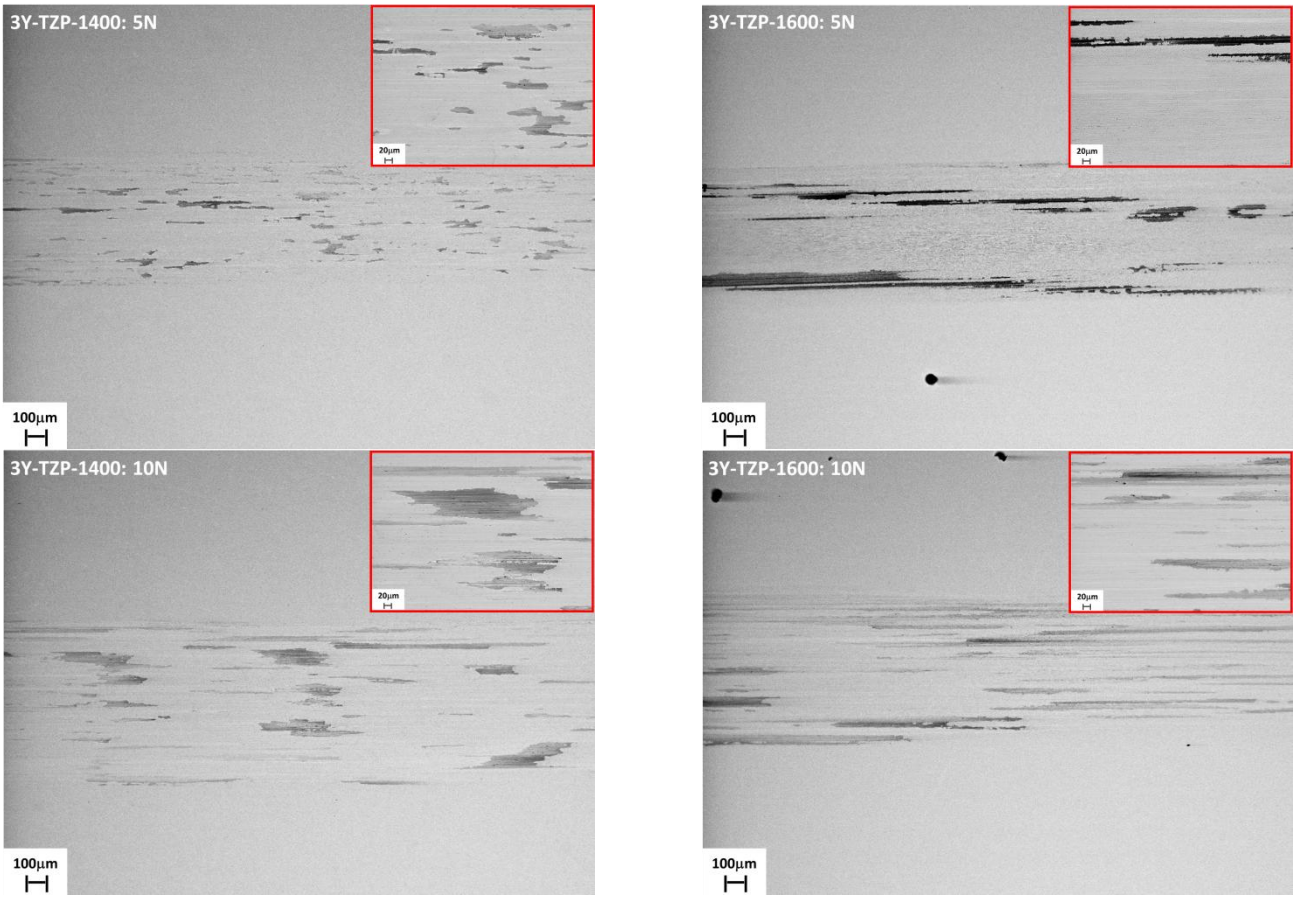


Figure 2. *Cont.*

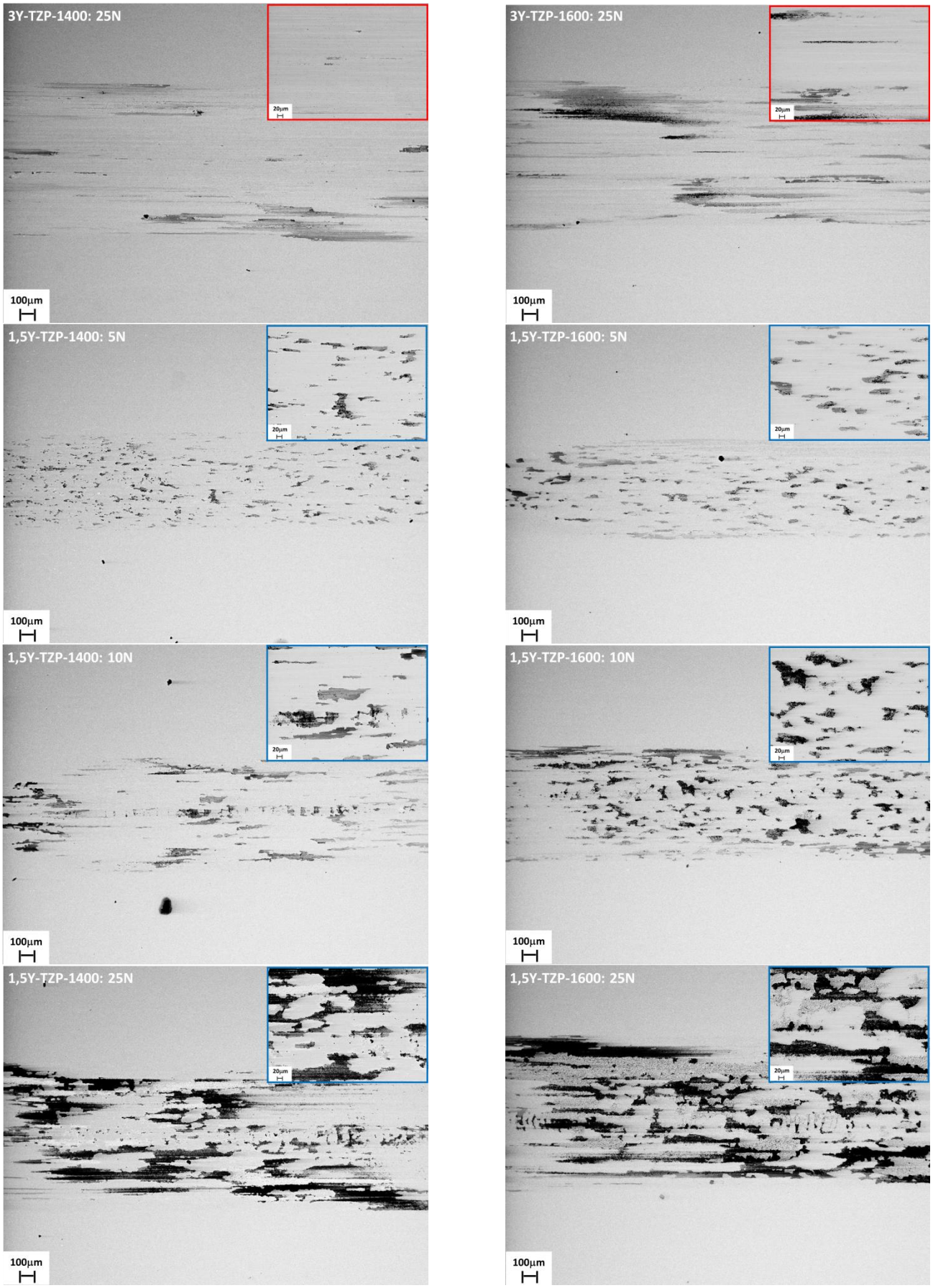


Figure 2. SEM micrographs illustrate typical wear tracks after the wear test with 5 N, 10 N, and 25 N applied loads for both of the tested materials at 1400 °C and 1600 °C.

3.5. Summary of Wear Mechanisms

For all studied materials and test conditions, the primary mechanism of wear was abrasive wear, strongly influenced by the transfer of SiC from the counterbody. The transferred SiC acted as a third-body abrasive medium. As the applied load increased, both the extent of SiC transfer and the severity of surface damage grew. In 1.5Y-TZP materials—particularly at 25 N—the transferred layer was extremely unstable, leading to fragmentation, delamination, and highly destructive wear. Despite the differences in fracture toughness, the SEM analysis of the wear tracks did not reveal evidence of extensive brittle fracture (e.g., large-scale spalling); wear appeared to be primarily governed by the abrasive mechanism and interaction with the transferred SiC.

4. Discussion

The results reveal a significant dependence of mechanical and tribological properties on both the yttria content and the SPS sintering temperature. This discussion is structured around the distinct behaviors of the two compositions and the underlying wear mechanisms, while also acknowledging the limitations of this study.

4.1. The Stable Performance of 3Y-TZP

For the standard 3Y-TZP composition, the mechanical properties showed remarkable stability across the tested temperature range. Both the microhardness (HV~1300) and fracture toughness (~4.2 MPa·m½) remained virtually unchanged between 1400 °C and 1600 °C. This suggests that near-full densification (>99%) and an optimal, fine-grained microstructure were already achieved at the lower sintering temperature of 1400 °C. The high yttria content effectively stabilizes the tetragonal phase, preventing significant grain growth or undesirable phase transformations even at 1600 °C under SPS conditions [2,14]. This inherent stability makes 3Y-TZP a robust and predictable material, where processing windows can be relatively broad without sacrificing core mechanical properties.

4.2. The Critical Temperature–Toughness Trade-Off in 1.5Y-TZP

In stark contrast, the 1.5Y-TZP composition was highly sensitive to the sintering temperature. The most critical finding of this study is the dramatic drop in fracture toughness from an exceptional ~6.2 MPa·m½ at 1400 °C to a modest ~4.5 MPa·m½ at 1600 °C. This >25% reduction strongly indicates a significant, detrimental change in the underlying microstructure. Based on the established literature, we hypothesize that this is caused by two related phenomena:

Excessive Grain Growth: Ceramics with lower stabilizer contents are known to be more susceptible to rapid grain growth at elevated temperatures [3,18]. It is likely that at 1600 °C, the grains in the 1.5Y-TZP sample grew beyond the critical size required for effective transformation toughening [9].

Spontaneous t→m Transformation: The slight decrease in bulk density observed for the 1.5Y-1600 sample (Table 1) provides further indirect evidence. This density drop is consistent with the occurrence of spontaneous tetragonal-to-monoclinic (t→m) transformation upon cooling. The associated ~4% volume expansion can introduce microcracks and porosity, thereby reducing both the density and fracture toughness [1,27].

The slight increase in the nanohardness and Young's modulus at 1600 °C for 1.5Y-TZP might seem counterintuitive but could be attributed to the intrinsic properties of the newly formed monoclinic phase, which, although detrimental to toughness, may possess higher stiffness.

4.3. Wear Mechanisms and the Role of Hardness vs. Toughness

The tribological tests revealed that under the tested conditions (dry sliding against a SiC ball), the primary wear mechanism was a combination of two-body abrasion and three-body abrasion mediated by material transfer from the SiC counterbody. The SEM analysis of the wear tracks (Figure 2) did not show evidence of large-scale brittle fracture or spalling, even in the toughest sample (1.5Y-1400). This suggests that for this tribosystem, hardness plays a more dominant role in resisting wear than fracture toughness.

This is supported by the low-load (5 N) results, where the harder 3Y-TZP samples exhibited significantly lower wear rates than the softer 1.5Y-TZP samples. As the load increased to 25 N, the formation of a thick, unstable tribolayer derived from the SiC counterbody became the dominant factor, leveling the wear performance across all samples. The lower hardness of 1.5Y-TZP likely facilitated the embedding of hard SiC debris, accelerating the three-body abrasive process.

4.4. Limitations and Future Work

The authors acknowledge several limitations in this study which open avenues for future research. Firstly, due to instrumental constraints, direct microstructural evidence (e.g., SEM of etched surfaces to quantify grain sizes) was not obtained, and phase analyses (e.g., XRD to confirm the t→m transformation) were not conducted. Therefore, the discussion on microstructural mechanisms remains hypothetical, albeit strongly supported by the mechanical data and established literature. Future work should prioritize this characterization to provide definitive confirmation.

Secondly, the use of different pressure profiles for the two sintering temperatures is a recognized confounding variable. While temperature is considered the dominant factor, a future study with identical pressure profiles would be valuable. Finally, the grayish color of the samples suggests potential minor carbon contamination from the graphite tooling, a common SPS artifact. Its influence on tribological performance warrants a more detailed chemical analysis in subsequent studies.

5. Conclusions

This study systematically investigated the influence of SPS temperature and yttria content on the mechanical and tribological properties of Y-TZP ceramics. The key findings lead to specific, application-oriented recommendations:

3Y-TZP is a robust, high-hardness material whose properties are insensitive to sintering temperatures between 1400 °C and 1600 °C. Its excellent wear resistance, particularly at lower contact stresses, makes it an ideal candidate for applications where surface durability is paramount, such as monolithic dental crowns, industrial bearings, and cutting tool inserts.

1.5Y-TZP is a high-toughness specialty material that is extremely sensitive to processing temperature. Sintering at 1400 °C produces a material with exceptional fracture toughness (~6.2 MPa·m½), making it suitable for safety-critical structural components where fracture prevention is the primary goal, such as load-bearing biomedical implants (e.g., femoral heads) or high-stress dental frameworks.

Increasing the sintering temperature to 1600 °C for 1.5Y-TZP is detrimental, causing a catastrophic loss of toughness. This is hypothesized to be due to excessive grain growth and spontaneous t→m transformation, highlighting the need for precise process control for low-yttria compositions.

Under dry sliding against SiC, wear is dominated by abrasion and material transfer, with hardness being a more critical factor for wear resistance than fracture toughness.

These conclusions underscore the critical importance of tailoring both the material composition and SPS processing parameters to achieve the desired balance of properties for a specific high-performance application.

Author Contributions: Methodology: D.M., J.A. and V.P.; validation: D.M.; formal analysis: D.M. and J.A.; investigation: D.M. and J.A.; data curation: D.M., J.A. and V.P.; writing—original draft preparation: D.M.; writing—review and editing: D.M.; visualization: J.A. and D.M.; supervision: D.M.; project administration: D.M.; funding acquisition: D.M. This manuscript, including related data, figures, and tables, has not been previously published and is not under consideration elsewhere. All authors have read and agreed to the published version of the manuscript.

Funding: This research was funded by EU NextGenerationEU through the Recovery and Resilience Plan for Slovakiagrant number [09I03-03-V04-00260].

Data Availability Statement: The original contributions presented in the study are included in the article, further inquiries can be directed to the corresponding author.

Conflicts of Interest: The authors have no competing interests to declare. The funding sources were not involved in the study's design, data collection or analysis, the preparation of this manuscript, or the decision to submit it for publication.

References

1. Palmero, P. Structural Ceramic Nanocomposites. A Review of Properties and Powders Synthesis Methods. *Nanomaterials* **2015**, *5*, 656–696. [CrossRef] [PubMed]
2. Stawarczyk, B.; Frevert, K.; Ender, A.; Roos, M.; Sener, B.; Wimmer, T. Comparison of four monolithic zirconia materials with conventional ones: Contrast ratio, grain size, four-point flexural strength and two-body wear. *J. Mech. Behav. Biomed. Mater.* **2016**, *59*, 128–138. [CrossRef] [PubMed]
3. Kulyk, V.; Duriagina, Z.; Kostryzhev, A.; Vasyliv, B.; Marenych, O. Effects of Sintering Temperature and Yttria Content on Microstructure, Phase Balance, Fracture Surface Morphology, and Strength of Yttria-Stabilized Zirconia. *Appl. Sci.* **2022**, *12*, 11617. [CrossRef]
4. Ouyang, J.H.; Sasaki, S.; Murakami, T.; Umeda, K. The synergistic effects of CaF_2 and Au lubricants on tribological properties of spark-plasma-sintered $ZrO_2(Y_2O_3)$ matrix composites. *Mater. Sci. Eng. A* **2004**, *386*, 234–243. [CrossRef]
5. Basu, B.; Vleugeles, J.; Van Der Biest, O. Microstructure–toughness–wear relationship of tetragonal zirconia ceramics. *J. Eur. Ceram. Soc.* **2004**, *24*, 2031–2040. [CrossRef]
6. Chevalier, J.; Gremillard, L.; Deville, S. Low-temperature degradation of zirconia and implications for biomedical implants. *Annu. Rev. Mater. Res.* **2007**, *37*, 1–32. [CrossRef]
7. Piconi, C.; Maccauro, G. Zirconia as a ceramic biomaterial. *Biomaterials* **1999**, *20*, 1–25. [CrossRef]
8. Lange, F.F. Transformation toughening: Part, I Size effects associated with the thermodynamics of constrained transformations. *J. Mater. Sci.* **1982**, *17*, 225–234. [CrossRef]
9. Garvie, R.C.; Hannink, R.H.; Pascoe, R.T. Ceramic steel? *Nature* **1975**, *258*, 703–704. [CrossRef]
10. Aktaş, B. Microstructure, Mechanical and Electrical Properties of CuO Doped 8YSZ. *High Temp. Mater. Process.* **2013**, *32*, 551–556. [CrossRef]
11. Ćorić, D.; Ćurkovič, L.; Renjo, M.M. Statistical Analysis of Vickers Indentation Fracture Toughness of Y-TZP Ceramics. *Trans. FAMENA* **2017**, *41*, 1–16. [CrossRef]
12. Ramachandra, M.; Abhishek, A.; Siddeshwar, P.; Vasanth, B. Hardness and Wear Resistance of ZrO_2 Nano Particle Reinforced Al Nanocomposites Produced by Powder Metallurgy. *Procedia Mater. Sci.* **2015**, *10*, 212–219. [CrossRef]
13. He, Y.J.; Winnubst, A.J.A.; Burggraaf, A.J.; Verweij, H. Sliding Wear of ZrO_2-Al_2O_3 Composite Ceramics. *J. Eur. Ceram. Soc.* **1997**, *17*, 1371–1380. [CrossRef]
14. Kulyk, V.; Duriagina, Z.; Vasyliv, B.; Vavrukh, V.; Kovbasiuk, T.; Lyutyy, P.; Vira, V. The Effect of Sintering Temperature on the Phase Composition, Microstructure, and Mechanical Properties of Yttria-Stabilized Zirconia. *Materials* **2022**, *15*, 2707. [CrossRef]
15. Palmeira, A.; Bondioli, M.; Strecker, K.; Santos, C. Densification and grain growth of nano- and micro-sized Y-TZP powders. *Ceram. Int.* **2016**, *42*, 2662–2669. [CrossRef]
16. Chevalier, J.; Cales, B.; Drouin, J.M. Low-temperature aging of Y-TZP ceramics. *J. Am. Ceram. Soc.* **1999**, *82*, 2150–2154. [CrossRef]
17. Kato, K.; Adachi, K. Wear of advanced ceramics. *Wear* **2002**, *253*, 1097–1104. [CrossRef]
18. Hannink, R.H.J.; Kelly, P.M.; Muddle, B.C. Transformation toughening in zirconia-containing ceramics. *J. Am. Ceram. Soc.* **2000**, *83*, 461–487. [CrossRef]

19. Kelly, J.R.; Denry, I. Stabilized zirconia as a structural ceramic: An overview. *Dent. Mater.* **2008**, *24*, 289–298. [CrossRef]
20. Gupta, T.K.; Bechtold, J.H.; Kunicki, R.C.; Cadoff, L.H.; Rossing, B.R. Stabilization of tetragonal phase in polycrystalline zirconia. *J. Mater. Sci.* **1977**, *12*, 2421–2426. [CrossRef]
21. Ji, M.; Xu, J.; Li, L.; Yu, D.; Chen, M.; El Mansori, M. Nano-scale mechanical behaviors and material removal mechanisms of zirconia ceramics sintered at various temperatures. *Ceram. Int.* **2021**, *47*, 32588–32598. [CrossRef]
22. Kozlovskiy, A.L.; Konuhova, M.; Borgekov, D.B.; Popov, A.I. Study of irradiation temperature effect on radiation-induced polymorphic transformation mechanisms in ZrO_2 ceramics. *Opt. Mater.* **2024**, *156*, 115994. [CrossRef]
23. Parveen, R.; Kalita, P.; Shukla, R.; Grover, V.; Pandey, R.; Sattonnay, G.; Avasthi, D.K. Investigation of radiation tolerance of yttria stabilized zirconia in the ballistic collision regime: Effect of grain size and environmental temperature. *Nucl. Instrum. Methods Phys. Res. Sect. B Beam Interact. Mater. At.* **2024**, *551*, 165344. [CrossRef]
24. *ISO 18754:2020*; Fine Ceramics—Determination of Apparent Density, Mass, and Porosity. International Organization for Standardization: Geneva, Switzerland, 2020.
25. Oliver, W.C.; Pharr, G.M. An improved technique for determining hardness and elastic modulus using load and displacement sensing indentation experiments. *J. Mater. Res.* **1992**, *7*, 1564–1583. [CrossRef]
26. Anstis, G.R.; Chantikul, P.; Lawn, B.R.; Marshall, D.B. A critical evaluation of indentation techniques for measuring fracture toughness: I, direct crack measurements. *J. Am. Ceram. Soc.* **1981**, *64*, 533–538. [CrossRef]
27. Chevalier, J. What future for zirconia as a biomaterial? *Biomaterials* **2006**, *27*, 535–543. [CrossRef]

Disclaimer/Publisher's Note: The statements, opinions and data contained in all publications are solely those of the individual author(s) and contributor(s) and not of MDPI and/or the editor(s). MDPI and/or the editor(s) disclaim responsibility for any injury to people or property resulting from any ideas, methods, instructions or products referred to in the content.